J Therm Anal Calorim (2010) 100:117–124
DOI 10.1007/s10973-009-0017-4

Some thermodynamic functions and kinetics of thermal decomposition of $NH_4MnPO_4 \cdot H_2O$ in nitrogen atmosphere

Chanaiporn Danvirutai · Pittayagorn Noisong · Sujittra Youngme

Received: 23 March 2009 / Accepted: 13 May 2009 / Published online: 10 June 2009

Abstract The ammonium manganese phosphate monohydrate ($NH_4MnPO_4 \cdot H_2O$) was found to decompose in three steps in the sequence of: deammination, dehydration and polycondensation. At the end of each step, the consecutive one started before the previous step was finished. The thermal final product was found to be $Mn_2P_2O_7$ according to the characterization by X-ray powder diffraction (XRD) and Fourier transform infrared spectroscopy. Vibrational frequencies of breaking bonds in three stages were estimated from the isokinetic parameters and found to agree with the observed FTIR spectra. The kinetics of thermal decomposition of this compound under non-isothermal conditions was studied by Kissinger method. The calculated activation energies E_a are 110.77, 180.77 and 201.95 kJ mol^{-1} for the deammination, dehydration and polycondensation steps, respectively. Thermodynamic parameters for this compound were calculated through the kinetic parameters for the first time.

Keywords Ammonium manganese phosphate monohydrate · Kinetics · Thermal decomposition · Thermodynamics

Introduction

The well known series of compounds of type $M^IM^{II}PO_4 \cdot H_2O$ ($M^I = K^+$, NH_4^+; $M^{II} = Mg^{2+}$, Mn^{2+}, Fe^{2+}, Co^{2+}, Ni^{2+}) relate to the dittmarite series. All of these compounds crystallize in the rhombic space group $Pmn2_1\left(C_{2v}^7\right)$ with $Z = 2$ [1]. These minerals are related to struvite ($NH_4MgPO_4 \cdot 6H_2O$), which is found on ivory and comes from the formation in urinary tracts and kidneys [2, 3]. Dittmarite series are reported to be a biomineral and found (rather infrequently) in urinary calculi [2]. They have been widely applied as fireproof materials, fertilizers, pigments for paints finishes for protection of metal and for extraction of divalent cations from sea-water [4–7]. They are a good source of macro- and micronutrients for plants [8]. Inorganic phosphate hydrates are transformed into various forms of phosphates or polyphosphates through the dehydration and hydrolysis reactions upon heating [9, 10]. Those metal polyphosphates have been used in the fields of luminescence and biomaterial ($Ca_2P_2O_7$) [11] and industrial catalyst ($(VO)_2P_2O_7$, $Mn_2P_2O_7$) [12, 13]. The thermal final decomposition product of various manganese phosphorous compounds e.g. $Mn(HPO_3)$ [14], $MnPO_4 \cdot H_2O$ [15] and $Mn(H_2PO_2)_2 \cdot H_2O$ [16] is found to be $Mn_2P_2O_7$, which exhibits interesting magnetic [17] and catalytic properties [18]. Despite the vibrational behavior of dittmarite series was widely studied in the literature [19], the thermal analysis of this series has received little attention. In this respect, they are of great interest to be selected for studying their kinetic and thermodynamic properties of thermal decomposition.

The thermogravimetric/derivative thermogravimetric/differential thermal analysis (TG/DTG/DTA) study is a universal technique and widely used for the measurements of kinetic parameters including the activation energy and preexponential factor of transformation processes, which involves chemical and physical changes in living biochemical metabolism, as well as in the fields of industrial and scientific researches. Besides, the thermodynamic parameters of activated complex can be calculated through

C. Danvirutai (✉) · P. Noisong · S. Youngme
Department of Chemistry and Center of Excellence for Innovation in Chemistry, Faculty of Science, Khon Kaen University, Khon Kaen 40002, Thailand
e-mail: chanai@kku.ac.th

kinetic parameters, which are important in theoretical study and applications in manufacturing level.

In our previous work, the kinetics and thermodynamic properties of phosphate hydrate compound had been studied [20] and the aim of this work was to synthesize $NH_4MnPO_4 \cdot H_2O$ and its transformation products, those were characterized by TG/DTG/DTA, Fourier transform infrared spectroscopy (FTIR) and X-ray diffraction (XRD). The non-isothermal decomposition kinetics analysis of $NH_4MnPO_4 \cdot H_2O$ in N_2 atmosphere was carried out using the isoconversional method of Kissinger [21]. The wavenumbers of the activated bonds of three activation steps were calculated and compared with the observed values from FTIR spectra. The kinetic parameters and estimated the thermodynamic functions of transition state complexes ($\Delta H^{\neq}$, $\Delta S^{\neq}$, $\Delta G^{\neq}$), kinetic (A, E) parameters as well as the calculated wavenumbers of the activated bonds in three decomposition steps of $NH_4MnPO_4 \cdot H_2O$ are discussed.

Experimental

Preparation

$NH_4MnPO_4 \cdot H_2O$ was prepared using a method reported in the literature [22]. A 0.5 M solution of $MnCl_2 \cdot 4H_2O$ was added to an excess saturated $(NH_4)_2HPO_4$ solution (10 M). Hydrazonium sulfate, $(N_2H_6)SO_4$ was added into a reaction mixture in order to prevent an aerobic oxidation of the divalent metal ion under an extremely basic condition. The prompt precipitation was obtained and was further digested at 358 ± 5 K for 1–2 days. Then the product was filtered, washed with DI water and dried in a desiccator.

Characterization

The manganese and water contents of synthesized $NH_4MnPO_4 \cdot H_2O$ were confirmed by using atomic absorption spectrophotometry AAS (Perkin-Elmer, Analyst 100) and TG/DTG/DTA (Pyris Diamond Perkin-Elmer). The TG/DTG/DTA experiments were performed at the heating rates of 10, 15, 20, and 25 K min^{-1} over the temperature range from 323 to 823 K in N_2 atmosphere with the flow rate of 100 mL min^{-1}. The sample mass of ca. 6.0–10.0 mg was filled into an aluminum crucible without pressing. The thermogram of a sample was recorded in an open aluminum pan using α-Al_2O_3 as the reference material. The synthesized $NH_4MnPO_4 \cdot H_2O$ was calcined in a thermal analyzer at 593 and 793 K in N_2 atmosphere and the thermal transformation products were further characterized. The morphologies of these compounds were investigated by SEM using LEO SEM VP1450 after gold coating. The FTIR spectra of the synthesized compound and its calcined samples were recorded in the range of 4000–370 cm^{-1} using KBr pellet technique (KBr, Merck, spectroscopy grade) on a Perkin-Elmer spectrum GX FTIR/FT Raman spectrophotometer with 16 scans and the resolution of 4 cm^{-1}.

The structures of the prepared hydrate and its calcined products were studied by XRD using a D8 Advanced powder diffractometer (Bruker AXS, Karlsruhe, Germany) with Cu $K\alpha$ radiation ($\lambda = 0.15406$ Å). The Scherrer method was used to evaluate the crystallite size (i.e. $D = K\lambda/\beta\cos\theta$, where λ is the wavelength of X-ray radiation, K is a constant taken as 0.89, θ is the diffraction angle and β is the full width at half maximum (FWHM)) [23].

Kinetics studies

The kinetic investigation of the non-isothermal decomposition for the dehydration of crystalline hydrates is a solid-state process of the type: A (solid) → B (solid) + C (gas) [24–26]. The kinetics of such reaction can be described by various equations taking into account the special features of their mechanisms. This is a model-free method, which involves measuring temperatures corresponding to the fix value of α (extent of conversion) at different heating rates (β).

All kinetic studies are assumed to be based on the following equations:

$$\frac{d\alpha}{dt} = kf(\alpha) \tag{1}$$

and

$$k = Ae^{-\frac{E}{RT}} \tag{2}$$

where $f(\alpha)$ is a function depending on the particular decomposition mechanism. The pre-exponential factor A (min^{-1}) is assumed to be independent of temperature (T/K), E is the activation energy (kJ mol^{-1}), R is the gas constant (8.314 J mol^{-1} K^{-1}), k is the rate constant and t is time. The combination of Eqs. 1 and 2 gives:

$$\frac{d\alpha}{dt} = Af(\alpha)e^{-\frac{E}{RT}}. \tag{3}$$

When β is the heating rate ($\beta = dT/dt$, K min^{-1}), Eq. 3 may be written as:

$$\frac{d\alpha}{dt} = \frac{dT\,d\alpha}{dt\,dT} = \beta\frac{d\alpha}{dT} = Af(\alpha)e^{-\frac{E}{RT}}. \tag{4}$$

Various methods of kinetic analyses are known such as Kissinger's method (differential method), Flynn–Wall–Ozawa [27, 28], Coats–Redfern [29] and Van Krevelen and Hoftijzer methods [30] (integral methods).

In kinetic study of $NH_4MnPO_4 \cdot H_2O$, Kissinger equation [21] was used to determine the activation energy and

preexponential factor of deammination, dehydration and polycondensation reactions. This method is well described and widely used in literature, which provides the reliable results.

The Kissinger equation used for E_α and A calculations is:

$$\ln\left(\frac{\beta}{T_P^2}\right) = \ln\left(\frac{AR}{E_\alpha}\right) - \left(\frac{E_\alpha}{RT_P}\right) \quad (5)$$

where E_α is the activation energy (kJ mol^{-1}), T_P is the peak temperature of the DTA curve which corresponds to the maximum reaction rate, while other parameters are the same as previously mentioned. The Arrhenius parameters, together with the reaction model, are sometimes called the kinetic triplet. According to Eq. 5, the plots of $\ln\left(\frac{\beta}{T_P^2}\right)$ against $\left(\frac{1000}{T_P}\right)$ can be obtained by a linear regression of least-square method. The activation energies E_α can be calculated from the slopes of the straight lines with the best linear correlation coefficient (r^2). Hence, the pre-exponential factor from a point of the maximum temperature, T_P can be calculated from the intercept of the straight lines.

Results and discussion

TG/DTG/DTA

Figure 1 shows the TG, DTG and DTA curves obtained at four heating rates (β = 10, 15, 20 and 25 K min^{-1}). The thermal decomposition of this compound exhibits three steps of mass losses, however step 1 is not well separated from step 2. The TG curves illustrate no change in mass of the compound until 423 K was attained. After that remarkable mass loss was observed. Three steps of mass losses correspond to three consecutive DTA endothermic peaks at the maxima of 505, 551 and 711 K for the heating rate of 10 K min^{-1}. The deammination and dehydration steps are observed as partially overlapping peaks over the range of 373–593 K. The polycondensation step is suggested to be observed over the range of 593–823 K. The final decomposition product was confirmed to be manganese pyrophosphate ($Mn_2P_2O_7$). The corresponding observed weight losses in two areas of decomposition were 18.85% and 5.20% by mass (Fig. 1), which agree very well with theoretical mass losses of 18.85% and 5.96%, respectively. The first and second steps of mass losses correspond to the co-elimination of ammonia and water molecules and the third corresponds to intramolecular dehydrations (polycondensations) of anion, which occurs until the completion of deammination and dehydration were attained. The mechanism for the thermal decomposition is suggested as follow [31]:

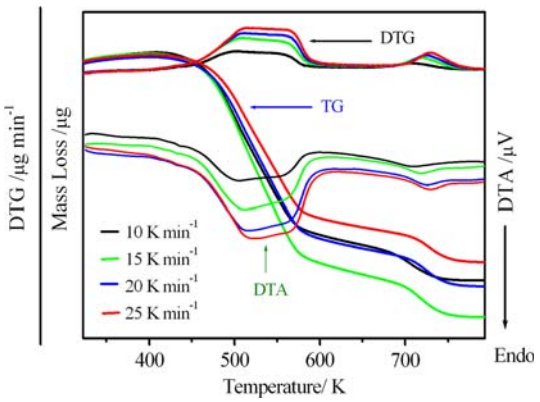

Fig. 1 TG/DTG/DTA curves of the synthesized $NH_4MnPO_4 \cdot H_2O$ at four heating rates of 10, 15, 20 and 25 K min^{-1} in N_2 atmosphere

Steps 1, 2 (in the range of 373–593 K)

$$NH_4MnPO_4 \cdot H_2O(s) \rightarrow MnHPO_4(s) + NH_3 \uparrow + H_2O \uparrow . \quad (6)$$

Step 3 (in the range of 593–823 K)

$$2MnHPO_4(s) \rightarrow Mn_2P_2O_7(s) + H_2O \uparrow . \quad (7)$$

SEM

The SEM micrographs of the title compound and its calcined products at 593 and 793 K in N_2 atmosphere are shown in Fig. 2. The particle shapes and sizes are found to change throughout the whole dehydration and decomposition products. The SEM micrograph of $NH_4MnPO_4 \cdot H_2O$ (Fig 2a) illustrates rod-like crystals, having sizes of about 1.00–2.00 μm in width and 4.00–5.00 μm in length. The calcined product at 593 K (Fig 2b) shows retexturing and coalescence in aggregates of irregularly non-uniform shape of different sizes in the wide range of 0.50–6.00 μm. The SEM micrograph of $NH_4MnPO_4 \cdot H_2O$ calcined at 793 K (Fig 2c) shows similar change as in Fig. 2b. The morphologies of calcined products are different from that of $NH_4MnPO_4 \cdot H_2O$, which is the effect of the deammination, dehydration and the polycondensation processes.

FTIR spectroscopy

The FTIR spectra of synthesized $NH_4MnPO_4 \cdot H_2O$ and its calcined products at 593 and 793 K are shown in Fig. 3a, b and c, respectively. The band at 3423 cm^{-1} in Fig. 3a is assigned to the O–H stretching vibration, while the bands below 3223 cm^{-1} in the FTIR spectra is due to the N–H stretches. The stretching vibrations of ammonium ion are observed in the region close to the OH stretching of water molecules in the range of 3400–2700 cm^{-1}. The overlapping of these bands causes the complicated vibrational spectrum. However, the vibrational frequencies of ammonium ion

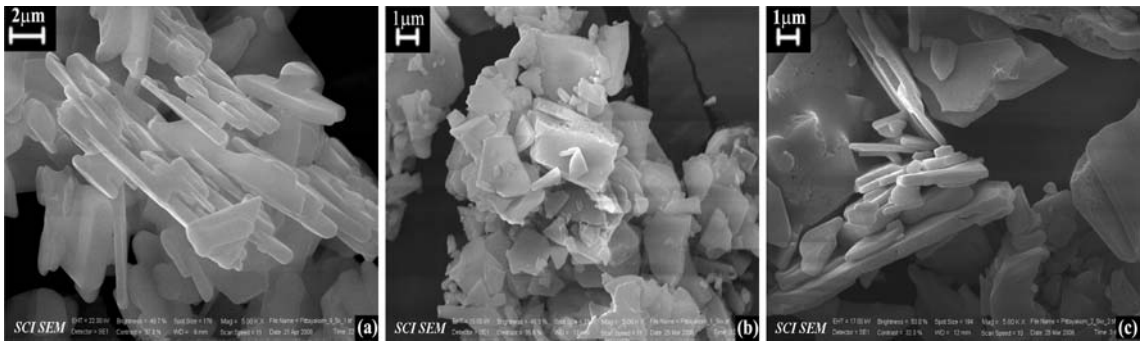

Fig. 2 SEM micrographs of synthesized $NH_4MnPO_4 \cdot H_2O$ (**a**) and its calcined products at 593 K (**b**) and 793 K (**c**) in N_2 atmosphere

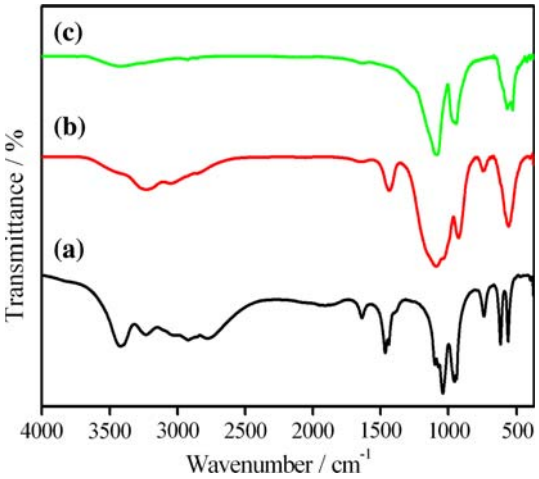

Fig. 3 FTIR spectra of the synthesized $NH_4MnPO_4 \cdot H_2O$ (*a*), the calcined $NH_4MnPO_4 \cdot H_2O$ in N_2 atmosphere at 593 K (*b*) and at 793 K (*c*)

appear at lower positions than those of the water molecules. The bands observed in the 1500–1300 cm^{-1} region are attributed to N–H bending vibrations. The phosphate ion vibrations are found in the range of 1008–931, 500–375, 1176–1015 and 630–510 cm^{-1} for $v_1(A_1)$, $v_2(E)$, $v_3(F_2)$ and $v_4(F_2)$, respectively.

The FTIR spectrum in the 1090–370 cm^{-1} region of the calcined $NH_4MnPO_4 \cdot H_2O$ at 593 K in N_2 atmosphere (Fig. 3b) shows characteristic of $MnHPO_4$ [32], while the calcined product at 793 K (Fig. 3c) exhibits the same characteristic as $Mn_2P_2O_7$ [33]. The FTIR bands are characterized based on the fundamental vibrating unit $P_2O_7^{4-}$ anion. The P–O stretching modes of the $[P_2O_7]^{4-}$ anion are known to appear in the 1250–975 cm^{-1} region [34–36]. The symmetric PO_2 stretching vibrations (v_{sym} PO_2) of $Mn_2P_2O_7$ samples are observed in the range of 1000–1100 cm^{-1}, while the asymmetric stretching vibrations (v_{asym} PO_2) appear in the range of 1100–1200 cm^{-1}. The asymmetric (v_{asym} POP) and symmetric stretching vibrations (v_{sym} POP) of POP bridge in this sample are observed in the 1000–900 and 700–400 cm^{-1} regions, respectively.

The authors demonstrated [37] based on the equation suggested by Vlase et al. [38] that the specificity of non-isothermal decomposition is due to the vibrational energy on a certain bond, which bases on anharmonic oscillation. Consequently, the wavenumber of the activated bond can be calculated from the isokinetic parameter T_i using [37–39]:

$$\omega_{calc} = \frac{k_B}{hc} T_i = 0.695\, T_i \tag{8}$$

and

$$\omega_{sp} = q\omega_{calc} \tag{9}$$

where k_B, h are the Boltzmann and Planck constants, c is the light velocity, q is the number of quanta ($q \in N$) and ω_{sp} is the assigned spectroscopic wavenumber for the bond supposed to be broken. T_i is the isokinetic temperature as related to the activation energy and preexponetial factor [40, 41]. In this work, we suggested to use the average maximum peak T_p in four heating rates to calculate ω_{calc} according to Eq. 8. The T_p values are 513.12, 558.24 and 720.95 K, which correspond to the first, second and third decomposition steps, respectively. The values of ω_{calc} for three steps can be further related to the ω_{sp} as given in Eq. 9 and the results are shown in Table 2. These data reveal that the oscillations of the N–H bonds in ammonium ion, O–H bonds in crystal water molecules and O–P–H of $MnHPO_4$ correlate with the elimination of NH_3, water (H_2O) of crystallization and an intramolecular dehydration in first, second and third steps, respectively. However, the small differences of average T_p and the wavenumber for the breaking bonds (ω_{calc}) for the first and second steps are affected by the co-elimination of an ammonia and a water of crystallization. The studied hydrate exhibits a very good agreement between the calculated wavenumber and the corresponding observed wavenumber in FTIR spectra.

X-ray powder diffraction

The XRD patterns of the synthesized $NH_4MnPO_4 \cdot H_2O$ and its calcined products at 593 and 793 K in N_2 atmosphere are shown in Fig. 4. All detectable peaks of the $NH_4MnPO_4 \cdot H_2O$ and the calcined products at 593 and 793 K in N_2 atmosphere are indexed as the synthesized $NH_4MnPO_4 \cdot H_2O$, $MnHPO_4$ and $Mn_2P_2O_7$ structures, those are identified using the standard data of PDF # 860577, PDF # 470199 and PDF # 771243, respectively. These results indicated that $NH_4MnPO_4 \cdot H_2O$ and $Mn_2P_2O_7$ crystallize in orthorhombic system with space group $Pmn2_1$ ($Z = 2$) and monoclinic system with the space group C2/m ($Z = 2$), respectively. In the case of $MnHPO_4$, the corresponding PDF standard file is not available. However, this structure is estimated to be the highly amorphous phase, which is confirmed by the PDF # 470199 for the case of $MnHPO_4 \cdot 2.25H_2O$ compound. The average crystallite sizes and lattice parameters of these compounds calculated from XRD patterns are tabulated in Table 1. The lattice parameters of $NH_4MnPO_4 \cdot H_2O$ and $Mn_2P_2O_7$ are compared with those reported in the standard data and found to agree well.

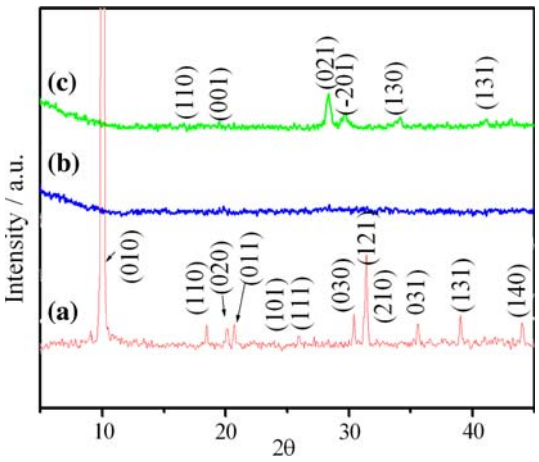

Fig. 4 XRD patterns of the synthesized $NH_4MnPO_4 \cdot H_2O$ (*a*), the calcined $NH_4MnPO_4 \cdot H_2O$ in N_2 atmosphere at 593 K (*b*) and at 793 K (*c*)

Kinetic and thermodynamic studies

Calculation of the activation energy and preexponential factor

The use of isocoversional or model-free methods (Kissinger, Ozawa and KAS) has increased recently due to the ability of these methods to calculate activation energy values without modelistic assumptions. In addition, the Kissinger method can be applied to calculate the preexponential factor, while the Ozawa and KAS methods can be used only to calculate the activation energy E values. Besides, the temperature corresponding to the maximum reaction rate (T_p) in Kissinger method can be used to estimate the wavenumber of the activated bond according to Eq. 8. The Kissinger plots according to Eq. 5 obtained from four DTA measurements are presented in Fig. 5. The calculated activation energies (E_α) and preexponential factor (A) with best linear correlation coefficient (r^2) were presented in Tables 2 and 3, respectively. The activation energy values of three steps were found to be 110.77, 180.77 and 201.72 kJ mol^{-1}, respectively, which reveal that the next step can occur harder than the previous step. However, the kinetic parameters (A and E) can be evaluated with different calculation procedures. The first and second steps exhibit lower activation energy in comparison with the third decomposition step. This is reasonable, because the third step corresponds to a covalent P–OH bond breaking. The small difference (20–70 kJ mol^{-1}) of

Table 1 Average particle sizes and lattice parameters of $NH_4MnPO_4 \cdot H_2O$ and calcined $NH_4MnPO_4 \cdot H_2O$ at 593 and 793 K in N_2 atmospheres calculated from XRD data

l	Method	*a*/Å	*b*/Å	*c*/Å	*β*/°	Average particle sizes (nm)
$NH_4MnPO_4 \cdot H_2O$	PDF # 860577	5.730	8.819	4.908	–	–
	This work	5.71(3)	8.81(5)	4.90(1)	–	47 ± 9
	DIF. PDF—this work	0.017	0.004	0.007	–	
$MnHPO_4$ $NH_4MnPO_4 \cdot H_2O$ calcined (320 °C)	PDF # 441319	Non-crystalline				
	This work	Non-crystalline				
	DIF. PDF—this work	Non-crystalline				
$Mn_2P_2O_7$ $NH_4MnPO_4 \cdot H_2O$ calcined (520 °C)	PDF # 771243	6.633	8.584	4.646	102.67	–
	This work	6.69(5)	8.55(0)	4.66(6)	102.88(4)	32 ± 8
	DIF. PDF—this work	−0.062	0.034	−0.02	−0.214	

— not detectable

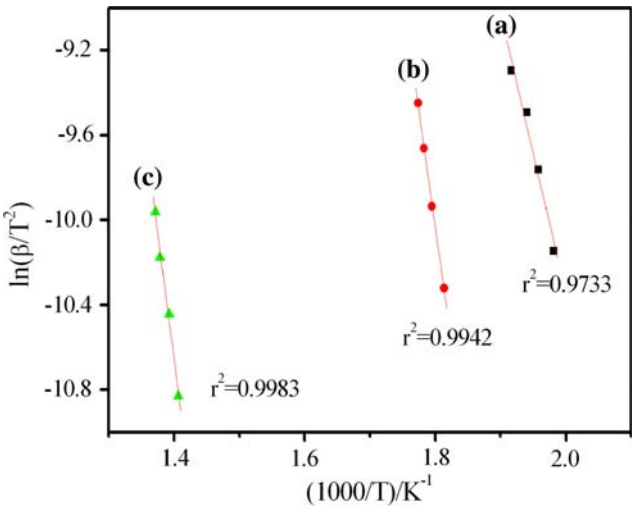

Fig. 5 Kissinger plots of the transformation due to the dehydration (*a*) deamination (*b*) and polycondensation (*c*) steps of $NH_4MnPO_4 \cdot H_2O$

activation energies in three transformation steps indicates that they are not completely separated [31], however the three maxima can be identified. The decomposition of $NH_4MnPO_4 \cdot H_2O$ under non-isothermal conditions, comprises of three non-separable steps: deammination, dehydration and polycondensation. The preexponential factors of three steps were found to be 1.59×10^{11}, 9.52×10^{16} and 3.2×10^{14} min^{-1}, respectively. These values reflect to the collision frequencies which reveal that the number of collision of molecules are in the sequence: step 2 > step 3 > step 1. The results can be interpreted in terms of the non-completely separable processes among the deammination, dehydration and decomposition (polycondensation) steps based on the comparable magnitude of the frequency factor (*A*).

Calculation of thermodynamic parameters

The pre-exponential factor or Arrhenius constant (*A*) can be calculated only by Kissinger method. The related thermodynamic functions can be evaluated by using the activated complex theory (transition state) of Eyring [42, 43]. The following general equation can be written [43]:

$$A = \left(\frac{e\chi k_B T_0}{h}\right) \exp\left(\frac{\Delta S^{\neq}}{R}\right) \tag{10}$$

where e is the Neper number ($e = 2.7183$), χ is the transition factor, which is unity for monomolecular reaction, k_B is the Boltzmann constant ($k_B = 1.3806 \times 10^{-23}$ J K^{-1}), h is Plank's constant ($h = 6.6261 \times 10^{-34}$ J s), T_0 is the peak temperature of the DTA curve (corresponding stage in the highest heating rate) and $\Delta S^{\neq}$ is the entropy change of transition state complex or entropy of activation. Thus, the entropy of activation may be expressed as follows:

$$\Delta S^{\neq} = R \ln \frac{Ah}{e\chi k_B T_0}. \tag{11}$$

The enthalpy change of transition state complex or heat of activation ($\Delta H^{\neq}$) and Gibbs free energy of activation ($\Delta G^{\neq}$) can be calculated according to Eqs. 12 and 13, respectively.

$$\Delta H^{\neq} = E^{\neq} - RT_0 \tag{12}$$

$$\Delta G^{\neq} = \Delta H^{\neq} - T_0 \Delta S^{\neq} \tag{13}$$

where $E^{\neq}$ is the activation energy E_a calculated from the Kissinger method. Thermodynamic parameters were calculated from Eqs. 11–13 and are summarized in Table 3. The positive values of $\Delta S^{\neq}$ for the second and third steps reveal that the activated state is highly disordered compared to the initial state. On the other hand, the negative

Table 2 Comparison between kinetic and spectroscopic data from Kissinger method

Step	Temperature/K in four heating rates/K min^{-1}				E_a/ kJ mol^{-1}	Average T_P/K	ω_{calc}/cm^{-1}	q	$q\omega_{calc}$/ cm^{-1}	ω_{sp}/cm^{-1} observed in FT/IR spectra	Assignment
	10	15	20	25							
1	504.78	510.68	515.26	521.75	110.77	513.12	356.62	9	3209	3235,3029	N–H bonds in ammonium ion
								8	2852	2924,2855	
								4	1426	1465,1438	
2	551.28	557.09	560.94	563.67	180.77	558.24	387.98	9	3492	3423	O–H in water of crystallization molecules
								8	3104	3235,3029	
								4	1552	1637	
3	711.08	718.27	725.41	729.04	201.72	720.95	501.06	2	1002	1040	P–O–H of $MnHPO_4$
								1	501	561	

Table 3 Values of $\Delta S^{\neq}$, $\Delta H^{\neq}$, $\Delta G^{\neq}$ and A for deammination, dehydration and polycondensation steps of $NH_4MnPO_4 \cdot H_2O$

Parameters	Deammination	Dehydration	Polycondensation
$\Delta S^{\neq}$/J mol^{-1} K^{-1}	−43.44	66.51	17.02
$\Delta H^{\neq}$/kJ mol^{-1}	106.43	176.08	195.66
$\Delta G^{\neq}$/kJ mol^{-1}	129.1	138.59	183.25
A/min^{-1}	1.59×10^{11}	9.52×10^{16}	3.2×10^{14}

value in the first step means that the activated complex has lower disorderness than the initial state. These $\Delta S^{\neq}$ values suggest a large number of degrees of freedom due to rotation and vibration which may be interpreted as a "fast" stage [43, 44] in dehydration and polycondensation steps, while deammination step can be interpreted as a "slow stage". The positive values of $\Delta G^{\neq}$ at all studied steps are due to the fact that, the deammination, dehydration and decomposition processes are not spontaneous. The positivity of $\Delta G^{\neq}$ is determined by a small activation entropy and a large positive activation enthalpy according to the Eq. 13. The results (Table 3) illustrate that the second and third decomposition steps occur harder than the first decomposition step. The endothermic peaks in DTA data agree well with the positive sign of the activation enthalpy ($\Delta H^{\neq}$). The calculated activation energy E_α values of three decomposition steps exhibit the increasing E_α values from steps 1 to 3. The same effect is also observed in $\Delta H^{\neq}$ values and can be interpreted that the last step need higher energy pathway than the early ones. These results correspond well with the calculated wavenumbers of the activated bonds.

Conclusions

$NH_4MnPO_4 \cdot H_2O$ decomposes in three steps and the final product is $Mn_2P_2O_7$. The polycondensation process was started before the early process in last steps of decomposition is finished and the co-decomposition is occurred over the range of 243–593 K. The kinetic study of thermal decomposition of this compound was carried out by Kissinger method. A correlation between the non-isothermal temperature from DTA data and the wavenumber from FTIR data of activated complex assigned to the breaking bond is possible to analyze the thermal sensitive part of a molecule, by means of an adequate processing of the thermal analysis data, in relation with the FTIR spectra. The activation entropy $\Delta S^{\neq}$, enthalpy $\Delta H^{\neq}$ and Gibbs free energy $\Delta G^{\neq}$ of three decomposition steps in $NH_4MnPO_4 \cdot H_2O$ can be calculated through kinetic parameters. The thermodynamic functions agree well with the thermal analysis data. The discussion about the activation energy, pre-exponential factor in relation to the change of activation entropy, enthalpy and Gibbs free energy of three decomposition steps of the title compound is reported for the first time.

Acknowledgements The authors would like to thank the Department of Chemistry, Faculty of Science and Department of Environmental Engineering (For XRD), Faculty of Engineering of Khon Kaen University for providing research facilities. The financial support from the Development and Promotion in Science and Technology Talents Project (DPST) and the Center of Excellence for Innovation in Chemistry (PERCH-CIC), Commission on Higher Education, Ministry of Education is gratefully acknowledged.

References

1. Carling SG, Day P, Visser D. Crytal and magnetic structures of layer transition metal phosphate hydrates. Inorg Chem. 1995;34:3917–27.
2. Šoptrajanov B, Stefov V, Kuzmanovski I, Jovanovski G, Lutz HD, Engelen B. Very low H–O–H bending frequencies. IV. Fourier transform infrared spectra of synthetic dittmarite. J Mol Struct. 2002;613:7–14.
3. Frost RL, Weier ML, Erickson KL. Thermal decomposition of struvite. J Therm Anal Calorim. 2004;76:1025–33.
4. Lapina LM. Metal ammonium phosphates and their new applications. Russ Chem Rev. 1968;37:693–701.
5. Barros N, Airoldi C, Simoni JA, Ramajo B, Espina A, Garcia JR. Calorimetric determination of the effect of ammonium-iron (II) phosphate monohydrate on Rhodic Eutrudox Brazilian. Spectrochim Acta. 2006;441:89–95.
6. Erskine AM, Grim G, Horning SC. Ammonium ferrous phosphate: a pigment for metal protective paint finishes. Ind Eng Chem. 1944;36:456–60.
7. Vol'fkovich SI, Remen RE. Ammonium phosphates of magnesium, zinc and iron. Chem Abstr. 1956;50:6243.
8. Yuan A, Wu J, Bai L, Ma S, Huang Z, Tong Z. Standard molar enthalpies of formation for ammonium/3d-transition metal phosphates $NH_4MPO_4 \cdot H_2O$ (M = Mn^{2+}, Co^{2+}, Ni^{2+}, Cu^{2+}). J Chem Eng Data. 2008;53:1066–70.
9. Onoda H, Nariai H, Moriwaki A, Maki H, Motooka I. Formation and catalytic characterization of various rare earth phosphates. J Mater Chem. 2002;12:1754–60.
10. Onoda H, Kojima K, Nariai H. Additional effects of rare earth elements on formation and properties of some transition metal pyrophosphates. J Alloys Compd. 2006;408:568–72.
11. Bian JJ, Kim DW, Hong KS. Microwave dielectric properties of $Ca_2P_2O_7$. J Eur Ceram Soc. 2003;23:2589–92.
12. van Smaalen S, Dinnebier RE, Hanson J, Gollwitzer J, Büllesfeld F, Prokofiev A, et al. High temperature behavior of vanadyl pyrophosphate $(VO)_2P_2O_7$. J Solid State Chem. 2005;178:2225–30.
13. Takita Y, Sano KI, Kurosaki K, Kawata N, Nishiguchi H, Ito M, et al. Oxidative dehydrogenation of iso-butane to iso-butene I. Metal phosphate catalysts. Appl Catal. 1998;A167:49–56.
14. Chung UC, Mesa JL, Pizarro JL, Jubera V, Lezama L, Arriortua MI, et al. $Mn(HPO_3)$: a new manganese (II) phosphite with a condensed structure. J Solid State Chem. 2005;178:2913–21.
15. Boonchom B, Youngme S, Maensiri S, Danvirutai C. Nanocrystalline serrabrancaite ($MnPO_4 \cdot H_2O$) prepared by a simple precipitation route at low temperature. J Alloys Compd. 2008;454:78–82.
16. Noisong P, Danvirutai C, Srithanratana T, Boonchom B. Synthesis, characterization and non-isothermal decomposition kinetics of manganese hypophosphite monohydrate. Solid State Sci. 2008;10:1598–1604.

17. Fowlis DC, Stager CV. Antiferromagnetic resonance in $Mn_2P_2O_7$. Can J Phys. 1972;50:2681–7.
18. Takita Y, Sano KI, Muraya T, Nishiguchi H, Kawata N, Ito M, et al. Oxidative dehydrogenation of iso-butane to iso-butene II. Rare earth phosphate catalysts. Appl Catal. 1998;170A:23–31.
19. Koleva VG. Metal–water interactions and hydrogen bonding in dittmarite-type compounds $M^IM^{II}PO_4 \cdot H_2O$ ($M^I = K^+$, NH_4^+; $M^{II} = Mn^{2+}$, Co^{2+}, Ni^{2+}): correlations of IR spectroscopic and structural data. Spectrochim Acta. 2005;62:1196–1202.
20. Boonchom B, Youngme S, Srithanratana T, Danvirutai C. Synthesis of $AlPO_4$ and kinetics of thermal decomposition of $AlPO_4 \cdot H_2O$–H_4 precursor. J Therm Anal Calorim. 2008;19:511–6.
21. Kissinger HE. Reaction kinetics in differential thermal analysis. Anal Chem. 1957;29:1702–6.
22. Basset H, Bedwell WL. Studies of phosphates. Part I. Ammonium magnesium phosphate and related compounds. J Chem Soc. 1993:854–71.
23. Cullity BD. Elements of X-ray diffraction. 2nd ed. Menlo Park: Addison-Wesley Publishing; 1978. p. 120.
24. Vlaev LT, Nikolova MM, Gospodinov GG. Non-isothermal kinetics of dehydration of some selenite hexahydrates. J Solid State Chem. 2004;177:2663–9.
25. Vyazovkin S. Computational aspects of kinetic analysis. Part C. The ICTAC kinetics project—the light at the end of the tunnel? Thermochim Acta. 2000;355:155–63.
26. Zhang KL, Hong JH, Cao GH, Zhan D, Tao YT, Cong CJ. The kinetics of thermal dehydration of copper(II) acetate monohydrate in air. Thermochim Acta. 2005;437:145–9.
27. Flynn JH, Wall LA. A quick direct method for the determination of activation energy from thermogravimetric data. Polym Lett. 1966;4:323–8.
28. Ozawa TA. New method of analyzing thermogravimetric data. Bull Chem Soc Jpn. 1965;38:1881–6.
29. Coats AW, Redfern JP. Kinetic parameters from thermogravimetric data. Nature. 1964;20:68–70.
30. Van Krevelens DW, Hoftijzer PJ. Kinetics of gas−liquid reaction-general theory. Trans I Chem E. 1954;32:5360–83.
31. Iqbal M, Bhuiyan H, Mavinic DS, Koch FA. Thermal decomposition of struvite and its phase transition. Chemosphere. 2008;70:1347–56.
32. Chapman AC, Thirlwell LE. Spectra of phosphorus compounds—I the infrared spectra of orthophosphates. Spectrochim Acta. 1964;20:937–47.
33. Steger E, Käßner B. Die infrarotspektren von wasserfreien schwermetall-diphosphaten. Spectrochim Acta. 1968; 24A:447–56.
34. Harcharras M, Ennaciri A, Rulmont A, Gilbert B. Vibrational spectra and structures of double diphosphates $M_2CdP_2O_7$ (M = Li, Na, K, Rb, Cs). Spectrochim Acta. 1997;A53:345–52.
35. Assaaoudi H, Butler IS, Kozinski J, Gariépy FB. Crystal structure, vibrational spectra and thermal decomposition of a new tetrazinc(II) dipyrophosphate decahydrate, $Zn_4(P_2O_7)$. J Chem Crystallogr. 2005;35:49–59.
36. Baril M, Assaaoudi H, Butler IS. Pressure-tuning Raman microspectroscopic study of cobalt(II), manganese(II), zinc(II) and magnesium(II) pyrophosphate dehydrates. J Mol Struct. 2005;751:168–71.
37. Boonchom B, Danvirutai D. Thermal decomposition kinetics of $FePO_4 \cdot 3H_2O$ precursor to synthetize spherical nanoparticles $FePO_4$. Ind Eng Chem Res. 2007;46:9071–6.
38. Vlase T, Vlase G, Doca M, Doca N. Specificity of decomposition of solids in non-isothermal conditions. J Therm Anal Calorim. 2003;72:597–604.
39. Pop N, Vlase G, Vlase T, Doca N, Mogos A, Ioitescu A. Compensation effect as a consequence of vibrational energy transfer in homogeneous and isotropic heat field. J Therm Anal Cal. 2008;92:313–7.
40. Mianowski A, Marecka A. The isokinetic effect as related to the activation energy for the gases diffusion in coal at ambient temperatures Part I. Fick's diffusion parameter estimated from kinetic curves. J Therm Anal Calorim. 2009;95:285–92.
41. Ioitescu A, Vlase G, Vlase T, Doca N. Kinetics of decomposition of different acid calcium phosphates. J Therm Anal Calorim. 2007;88:121–5.
42. Rooney JJ. Ering transition-state theory and kinetics in catalysis. J Mol Catal A. 1995;96:L1.
43. Boonchom B. Kinetics and thermodynamic properties of the thermal decomposition of manganese dihydrogenphosphate dihydrate. J Chem Eng Data. 2008;53:1533–8.
44. Vlaev L, Nedelchev N, Gyurova K, Zagorcheva M. A comparative study of non-isothermal kinetics of decomposition of calcium oxalate monohydrate. J Anal Appl Pyrol. 2008;81:253–62.